COMMUNICATIONS IN SCIENCE AND TECHNOLOGY
Homepage: cst.kipmi.or.id

Modification of Chitosan/PEG4000 dispersed with Lithium Triflate ($LiCF_3SO_3$) as a solid polymer electrolyte for the secondary battery

Kartika Sari[a,*], Arifin Nur Muhammad Haryadi[a], Nur Khusaenah[a], Sudaryanto[b], Evi Yulianti[b], Agung Bambang Setio Utomo[c]

[a]*Department of Physics, Universitas Jenderal Soedirman, Purwokerto 53123, Indonesia*
[b]*National Research and Innovation Agency (BRIN), Puspiptek Region, Serpong 15314, Indonesia*
[c]*Department of Physics, Universitas Gadjah Mada, Yogyakarta 55281, Indonesia*

Article history:
Received: 8 August 2024 / Received in revised form: 15 October 2024 / Accepted: 27 October 2024

Abstract

Secondary battery solid electrolytes attract researchers' attention for being one of the components of the anode and cathode separation in batteries. Currently, battery electrolytes on the market are liquid-based, which have weaknesses in their safety and are not environmentally friendly. Solid-based electrolytes can be a good choice since they excel in the safety and stability of mechanical and electrical properties; however, they still have the disadvantage of low conductivity values (~10^{-4} - 10^{-6} S/cm), thus requiring modification. The solid electrolytes modification using chitosan can be done by adding other polymers and salts as fillers and Li+ ion-making agents. This scientific paper offers an overview of the development of chitosan-based secondary battery solid electrolytes with the addition of PEG4000 polymer and $LiCF_3SO_3$. The study was conducted using the solution casting method producing solid electrolytes in the form of membranes. The addition of PEG4000 and $LiCF_3SO_3$ affected the microstructure and electrical permittivity of the polymer solid electrolyte membrane. PEG4000 as a plasticizer had no significant effect on inter- and intra-molecular bonds due to poor membrane homogeneity; meanwhile, $LiCF_3SO_3$ could increase the permittivity and ionic conductivity of the chitosan polymer solid electrolyte membrane to 3.199 x 10^{-7} S/cm. The chitosan polymer solid electrolyte membrane with the addition of PEG4000 and 30% $LiCF_3SO_3$ salt has an optimal value compared to other salt concentration variations. The results of this research concluded that $LiCF_3SO_3$ is evenly dispersed in the chitosan/PEG4000 solid polymer electrolyte membrane enabling it to be used as a secondary battery solid electrolyte.

Keywords: Solid electrolyte; secondary battery; crystal structure; permittivity; dielectric

1. Introduction

Battery technology is one of the key components in the development of new and renewable energy in Indonesia. The use of intermittent energy sources requires batteries as energy storage devices. One of the energy sources that require battery technology is solar and wind resources. Batteries are energy storage technologies that use electrochemical principles to produce constant voltage from chemical reactions [1]. The electrical energy produced by batteries comes from oxidation and reduction reactions. The battery has a number of main components, including anode, cathode, and electrolyte. Here, electrolyte is an important component in secondary batteries to prevent a direct contact between electrodes which function as a medium for ion flow between electrodes [2]. An ideal solid electrolyte battery has chemical stability, thermal stability, high proton conductivity, high flexibility, low cost, and abundant availability of materials in nature[3-4].

* Corresponding author.
Email: kartika.sari@unsoed.ac.id
https://doi.org/10.21924/cst.9.2.2024.1496

To develop solid battery electrolytes, previous researchers have developed various types of materials, one of which is chitosan, a type of natural polymer, as a solution for the composition of solid battery electrolytes [5]. The small size of chitosan particles has made it simple to be modified other chemical materials [6]. However, since chitosan itself is an insulator, the modification and improvement of electrical properties must be carried out to increase ionic conductivity. Chemicals for modifying chitosan include Polyethylene Oxide (PEO) and Polyethylene Glycol (PEG) [7]. PEO and PEG, which are in the form of white powder are easily soluble in water, methanol, and hydrophilic. They are polymer materials from ethylene oxide that can act as plasticizers.

Plasticizers are able to reduce the number of active centers and thus weaken the intermolecular and intramolecular forces between polymer chains [8]. This then results in a reduction in the stiffness of the three-dimensional structure and changes the mechanical and thermomechanical properties of the prepared film. The addition of a plasticizer with a low molecular weight can reduce the glass transition temperature (Tg) of the polymer electrolyte system. At this point, the reduction in crystallinity

and increase in salt dissociation ability is guaranteed [9].

Chitosan has an original isolator property, so it is modified and improved electrical properties to improve ionic conductivity [10]. PEG4000, meanwhile, can also conduct ions at room temperature. Chitosan and PEG4000 can be synthesized into a solid polymer membrane [11]. The addition of PEG4000 as a plasticizer with a high dielectric constant also has a significant role in increasing ionic conductivity by inducing ion dissociation and facilitating ion transportation. To increase the electrical properties of the chitosan/PEG4000 membrane, lithium triflate ($LiCF_3SO_3$) is used as a surfactant [12]. The amorphous or crystal properties of a material can be attributed to the value of the conductivity.

The increased conductivity and electrical properties of the chitosan/PEG4000 membrane-dispersed lithium triflate ($LiCF_3SO_3$) in this study are expected to qualify as a secondary battery application. In this study, chitosan as the primary ingredient, PEG4000 as a plasticizer, and lithium triflate salts ($LiCF_3SO_3$) as dopants were used as the material solutions. The study aims to determine the crystal structure and electrical properties of the solid polymer electrolyte (SPE) membrane.

2. Materials and Methods

The chitosan was purchased from Biotech Surindo (Cirebon, Indonesia) with a deacetylation degree (DD) of about 85%. Acetic acid (CH_3COOH from Merck, Polietilen Glikol (PEG) 4000, and Lithium Triflate ($LiCF_3SO_3$) were purchased from Sigma Aldrich. The research is divided into 2 stages: the solid polymer electrolyte (SPE) membrane synthesis stage and the characterization stage using Electrochemical Impedance Spectroscopy (EIS), X-Ray Diffraction (XRD), and Fourier Transform Infrared **(**FTIR) as shown in Fig. 1.

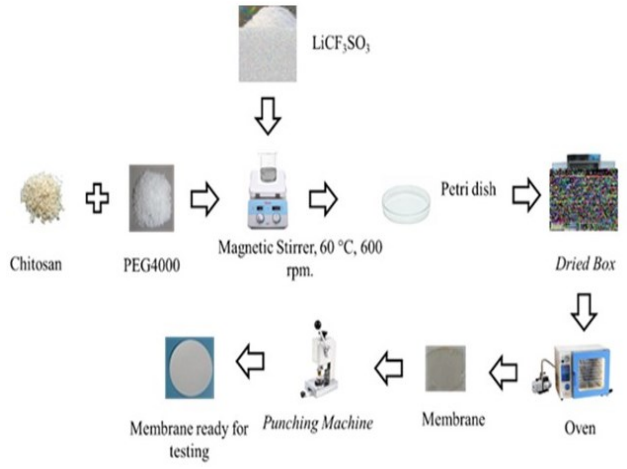

Fig. 1. Research Design

Fig. 1 shows the preparation of the SPE membrane samples. Chitosan ($C_6H_{11}NO_4$), PEG4000, Lithium Triflate ($LiCF_3SO_3$), Acetic acid (CH_3COOH 1%), and distilled water were used as media for mixing precursors. The preparation of chitosan/PEG4000/$LiCF_3SO_3$ solid polymer electrolyte (SPE) membranes was conducted through the solution casting method.

The chitosan, PEG4000, and various concentrations of $LiCF_3SO_3$ were gradually dissolved in CH_3COOH solution in a beaker using a hot plate magnetic stirrer at a speed of 600 rpm and at a temperature of 60ºC for 2 hours until being homogeneous. The variations in LiC_3SO_3 concentration were at 10%, and 30%. The homogeneous solution subsequently was poured into a petri dish and put into a drying machine and vacuum oven until it became a thin membrane with a diameter of 1.4 cm. The samples in this study included S1 (chitosan), S2 (Chitosan/PEG4000), S3 (Chitosan/PEG4000/$LiCF_3SO_3$ 10%), and S4 (Chitosan/PEG4000/$LiCF_3SO_3$ 30%) membranes.

2.1. Fourier transform infrared (FTIR)

Fourier Transform Infrared (FTIR) spectra were recorded on Shimadzu 8201 PC FTIR spectrophotometer and recorded with 1 cm^{-1} resolution in the transmission mode with the wavenumber range of 400 to 4000 cm^{-1}. The membranes were blended as a KBr pellet and scanned into a blank KBr pellet prior to measurement.

2.2. X-ray diffraction (XRD)

The XRD patterns were performed using X-ray Diffraction (XRD) type Rigaku D/max 2500 V diffractometer (Rigaku, Japan) with the Cu-Kα radiation (λ = 1.54060 Å), 40 kV, 30 mA, divergence slit/scattering slit, 0.3 mm receiving slit. The relative intensity was recorded in a scattering angle range (2θ) in the range of 10 – 800 with a scintillation counter at a scanning speed of 0.0020/min. The diffraction was smoothed by 75 points using Origin 10 software before calculating the relative crystallinity index of the solid polymer electrolyte membrane. The highest intensity of the diffractogram peak was used to calculate the crystallite size using Equation (1) (the Debye-Scherer Equation) [13-14].

$$D = \frac{\kappa\lambda}{\beta \cos\theta} \quad (1)$$

D is the crystallite size (nm), K is the Scherer constant (0.9), β is full-width half maximum peak (radians), λ is the wavelength of X-ray source with Cu k-α (1.5406 nm), and θ is diffraction angle.

2.3. Electrochemical impedance spectroscopy

The permittivity and dielectric properties of the solid polymer electrolyte membranes were pelletized into 15-mm spherical forms using 15 Mpa uniaxial pressures. Impedance spectra were collected at an applied 1 V and the frequency range of 42 Hz – 5 MHz using HIOKI LCR HiTESTER 3532-50. The complex dielectric constant and dielectric loss can be calculated by the equation [15]:

$$\varepsilon' = \frac{Z_r}{\omega Co(Z_r^2 + Z_i^2)} \quad (2)$$

$$\varepsilon'' = \frac{Z_i}{\omega Co(Z_r^2 + Z_i^2)} \quad (3)$$

where $C_o = \varepsilon_o A/t$, ε_o is the permittivity of free space, A is the

surface area, t is the thickness of the pellet, $\omega = 2\pi f$ (f is frequency), Z_i is the imaginary part of the complex permittivity, Z_r is the real part of the complex permittivity, ε' is the real part of the dielectric constant, and ε'' is the imaginary part of the dielectric loss.

3. Results and Discussion

A number of experiments have produced the SPE membrane. Fig. 2 illustrates four samples in the form of circular membrane with a diameter of 1 cm.

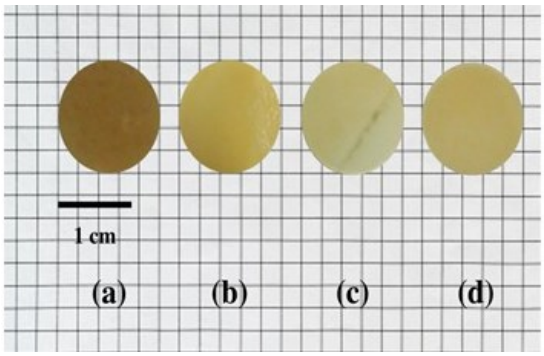

Fig. 2. The membrane (a) S1, (b) S2, (c) S3, (d) S4

Fig. 2 shows the samples of SPE membrane. The resulting solid electrolyte membranes had a thickness of between 0.363 and 0.5 mm. The membrane surface morphology looked smooth with a color that tended to be yellow due to the influence of chitosan as a polymer host. The S2, S3, and S4 membranes were not transparent in contrast to the chitosan membrane. Here, the transparent S3 and S4 membranes had a more elastic texture than that of the S2 membrane. The addition of $LiCF_3SO_3$ salt and PEG4000 plasticizer to the chitosan membrane increased the thickness of the membrane. Plasticizer is a colorless and odorless ester compound that is used to increase the elasticity of a material. The addition of plasticizers to the membrane material is expected to reduce intermolecular bonds between chitosan molecules, thereby weakening intermolecular forces [16].

3.1. Fourier transform infra-red (FTIR) spectroscopy

The excited atoms will form vibration patterns called as spectra. The spectrum of the materials contained in the sample varies in accordance to its composition to confirm the formation of complex compounds between the polymer matrixes. The complexation of the compounds formed is critical information in that the movement of internal charges through the polymer matrix is facilitated by the association of charge carriers with the polymer chain [17]. Fig. 3 shows the spectra results of S1, S2, S3, and S4 polymer membranes.

Fig. 3 depicts the presence of O-H stretching functional groups and overlap with N-H stretching functional groups at a wave number of 3425 cm^{-1} for S1 and S2 membranes. Stretching vibration refers to the movement of atoms or molecules that occurs regularly. The difference in wave number values in the types of vibrations occurred can be caused by the influence of the addition of PEG4000 as a plasticizer so that atomic interactions occur in the polymer membrane [18]. The addition of lithium triflate doping to the chitosan/PEG4000 polymer membrane also affects the absorption peak due to the interaction of atoms in lithium triflate with atoms from the host polymer [19]. In this study, the O-H stretching vibration that overlapped with N-H stretching in the chitosan/PEG4000/$LiCF_3SO_3$ polymer membrane occurred at a wave number of 3442 cm^{-1}. The phenomenon of O-H stretching vibrations overlapping with N-H stretching is one of the special characteristics of chitosan-based polymers [20].

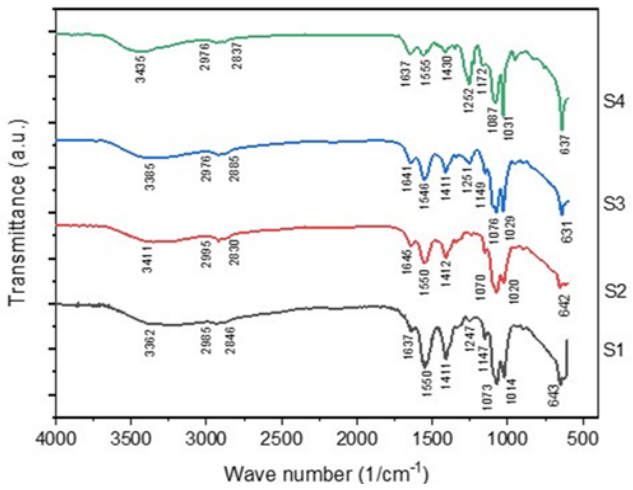

Fig. 3. FTIR spectra of S1, S2, S3, and S4 membranes

The addition of $LiCF_3SO_3$ to the host polymer membrane, (S1) can increase the intensity of the absorption peaks. Meanwhile, increasing the absorption intensity can increase the conductivity value of the polymer membrane in view of the higher free ions moving on the polymer membrane. The previous research showed that O-H bending was formed at wave numbers 3500 cm^{-1} [21]. CH_2 stretching vibrations occurred at wave numbers 2920 cm^{-1}, 2924 cm^{-1}, and 2929 cm^{-1}. The C-H stretching functional group was also formed at wave numbers 2879 cm^{-1}, 2854 cm^{-1}, and 2872 cm^{-1}. When $LiCF_3SO_3$ is added to the polymer membrane, there will be an interaction between the salt ions and the polymer membrane; hence, a shift in wave numbers occurs. The C=O functional group was formed at the wave numbers of 1642 cm^{-1}, 1644 cm^{-1}, and 1639 cm^{-1}, respectively. The formation of the C=O functional group in the range of 1650-1600 cm^{-1} is a characteristic of chitosan in polymer membranes. The shift in the wave number value can occur due to the interaction between atoms in each membrane [22].

The CH_2 wagging and CH_2 bending functional groups occurred at the wave numbers 1411 cm^{-1} for each polymer membrane. At the wave numbers 1343 cm^{-1} and 1352 cm^{-1}, the vibrations of the C-H bending functional group occurred. However, the vibration of the C-H bending functional group did not occur in the chitosan polymer membrane, indicating that the addition of plasticizer and lithium triflate salt can result in the emergence of a new absorption peak [23]. Bending vibration is the movement of atoms that causes changes in the bond angle between two bonds or the movement of a group of atoms towards other atoms [24].

The absorption peaks at wave numbers 1075 cm^{-1}, 1072 cm^{-1}, and 1077 cm^{-1} indicate the formation of vibrations of the C-O and NH_3^+ (amide) functional groups. Amide vibrations at wave numbers 1070 - 1080 cm^{-1} are also the characteristic of chitosan [25]. Vibrations in the fingerprint area occur at wave numbers 641 - 657 cm^{-1}, forming C-C stretching functional groups. The absorption peak formed in the fingerprint area forms a sharp peak. Molecular vibrations in polymer membranes added with lithium triflate have characteristics when compared to polymer membranes that are not doped with lithium triflate [26]. The type of vibration that occurs is the asymmetric vibration of SO_3 which is part of the anion ($CF_3SO_3^-$) at a wave number of 1262 cm^{-1}. The CF_3^- CF_3^- stretching functional group also occurs at a wave number 1164 cm^{-1}, while SO_3 is symmetric at wave numbers 1027 cm^{-1} and 641 cm^{-1}. This type of vibration does not occur in S1 polymer membranes without doping lithium triflate [27].

3.2. X-ray diffraction (XRD)

The characterization of the structure and crystal phase formed from the membranes was carried out using XRD in the 2θ range between 5°and 80°. Polymers with an amorphous phase had many empty cavities that allowed ions to move better than crystalline polymers. Crystalline polymers with a dense and regular structure can reduce the ions' movement in the crystal lattice and cause lower ionic conductivity [28]. Fig. 4 presents the XRD results of the membranes.

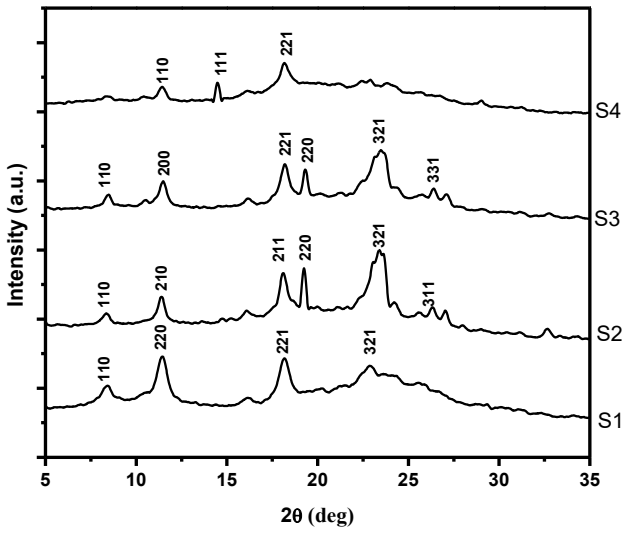

Fig. 4. The XRD diffractogram of S1, S2, S3, and S4 membranes

Fig. 4 shows the XRD diffractogram observed for the diffraction peak of S1 including (110), (220), (221), and (321) planes. The diffraction peak of S2 had (110), (210), (211), (220), (221), and (311) planes. For S3, the planes included (110), (200), (221), (310), (321), and (331), while for S4, they included (110), (111), and (210). The highest peak was at a diffraction angle of S1, S2, S3, and S4 with 11.42°, 23.34°, 18.22°, and 14.47°, respectively. The addition of PEG4000 had a significant effect on the change of crystal phase to be amorphous. A higher peak when chitosan was added to PEG4000 and $LiCF_3SO_3$ was determined by the uneven membrane surface. An uneven membrane surface can be caused by the agglomeration phenomenon in which particles can easily agglomerate when added to the polymer matrix. Agglomeration can occur during the process of forming materials or particles and when combined with other materials [29].

The agglomeration occurred can produce a crystal phase in the material. $LiCF_3SO_3$ salt on the membrane does not have a significant effect on phase changes. Several relatively sloping peaks after the addition of $LiCF_3SO_3$ salt indicate that the salt affects the phase change to a semicrystalline phase [30]. The crystallinity degree can be identified by comparing the crystal fraction and the area of the crystal and amorphous fractions [31-32]. Fig. 5 depicts the crystallinity degree of the S1, S2, S3, and S4 membranes.

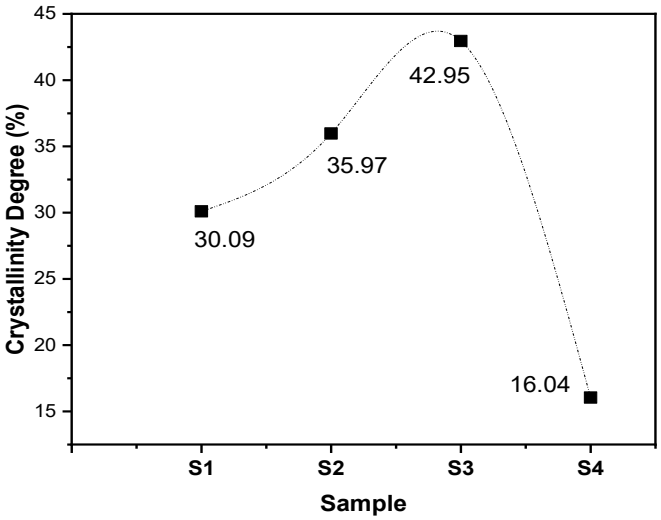

Fig. 5. The crystallinity degree of S1, S2, S3, S4 membranes

Fig. 5 shows the highest crystallinity degree obtained in the S1, S2, S3, and S4 including 30.09%, 35.97%, 42.95%, and 16.04%, respectively. The relationship between crystallinity degree and X-ray diffraction (XRD) peaks is related to a higher crystallinity degree in which the stronger XRD peaks are in view of increased crystalline order, while the weaker peaks are in view of decreased crystallinity. As crystallinity increases, the sharpness and intensity of the peaks inside the sample also can improve. The diffraction peaks disappear, the peak intensity decreases and the peak becomes wider showing the formation of complex compounds between chitosan and respective lithium salts. In addition, this phenomenon also shows that the addition of lithium salts can cause the chitosan structure to be increasingly amorphous, which can be related to changes in its ionic conductivity and structural properties.

The addition of PEG4000 had not a significant effect on the degree of crystallinity of the S1 membrane compared to the addition of $LiCF_3SO_3$ which had a significant effect on the crystallinity degree. PEG4000 produced a widening and decreasing crystal peak at the 2θ peak position. The effect of adding PEG4000 and $LiCF_3SO_3$ improved the battery performance as shown in Fig 6. The lattice strain can be caused by crystal defects that will affect the ionic conductivity. Membranes with large crystal defects will expand the ion transfer area [33].

Fig. 6 depicts the results of XRD for the membrane phase

structure showing the strain. Peak widening is known to produce two important effects: a decrease in crystallite size and the emergence of lattice strain [34]. The highest crystallite size produced by the S4 membrane was at 13.29 nm, while the smallest one was produced by the S1 membrane at 7.77 nm. The particle size is related to the width and half height of the peak (FWHM). The greater the FWHM value, the smaller the resulting crystallite size. Sample S1 had a small particle size caused by the 2θ angle that had a widened polymer peak. The large particle size was caused by sample S4 that had the sharp membrane diffraction peaks due to the addition of $LiCF_3SO_3$, making the particle size larger. This indicated the interaction of Li^+ ions with cations from the S2 membrane enabling an attractive bond to occur between crystals and cause the crystal diameter to be larger.

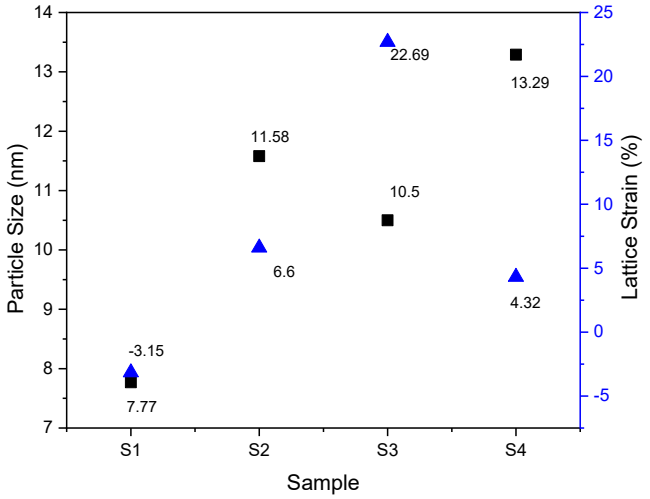

Fig. 6. Particle size and Lattice strain of S1, S2, S3, and S4 membranes

The effect of lattice strain is critical in the electrochemical performance of lithium battery devices [35]. Many studies have shown that the presence of lattice strain is the main cause of cracks that cause failure in material utilization. Other studies have shown that interfacial strain modifies lithium diffusion, thereby affecting interfacial resistance. Lattice strain occurs due to phase changes during the membrane synthesis process resulting in large crystal defects, later on, affecting the ionic conductivity value. This can occur as the membrane with large crystal defects will expand the ion transfer area. In this study, the largest lattice strain was found on the S3 membrane A at 22.68%, which could provide the largest space in each cell unit; hence, the largest possible polymer matrix bond length resulted in smooth Li^+ ion movement and increased the membrane ionic conductivity value. While, the lattice strain on the S4 membrane had a low lattice strain value of 4.32% indicating reduced crystal defects in the membrane, thus affecting the ionic conductivity value to be low.

3.3. Electrochemical impedance spectroscopy (EIS)

AC conductivity characterization was carried out to determine the ionic conductivity value of the solid electrolyte membrane. Fig. 7 presents the AC conductivity results of the membranes.

Fig. 7 shows the increase with increasing frequency value. AC conductivity on the S1 membrane had the highest value compared to the solid electrolyte membrane with the addition of PEG4000 and $LiCF_3SO_3$. The analysis of the amount of ion transfer was carried out to determine the polarization current of ions, both cations and anions in a material produced due to the response to the given potential difference [36]. The results of the AC conductivity curve were then fitted to determine the DC conductivity value in the plateau or horizontal area [37]. The AC conductivity graph fitting process is shown in Fig. 8 (a), (b), (c), and (d).

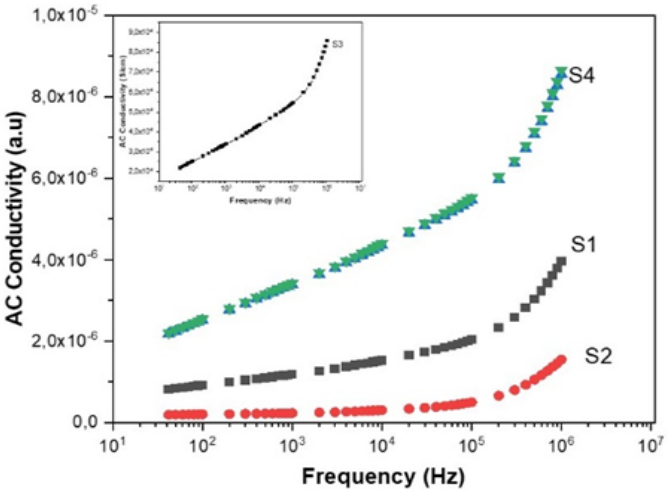

Fig. 7. AC Conductivity of S1, S2, S3, and S4 membranes

Fig. 8 shows the DC conductivity of S1, S2, S3, and S4 membranes. The ionic conductivity of S1, S2, S3, and S4 membranes included 9.351 x 10^{-9}, 5.025 x 10^{-11}, 3.45 x 10^{-7}, and 3.199 x 10^{-7} S/cm, respectively. The highest ionic conductivity was obtained in S3 and S4 membranes, while the lowest one was found in the S2 membrane. The increase in ionic conductivity can occur due to the phase transition of the polymer complex from the crystalline phase to semicrystalline or amorphous, and an increase in the concentration of charge carriers, and plasticizers can increase the volume in the electrolyte system [38]. The insignificant change in conductivity can be caused by the increase in bulk resistivity as shown in Fig. 9.

Fig. 9 illustrates that the electrolyte membrane has a semicircular curve pattern and is continued with a straight line. The Nyquist plot pattern shows how the membrane works as a conductor of charged material when given a load or a potential difference occurs [39]. The semicircular shape on the impedance graph in the battery system is related to the phase structure in the material and can be represented by an equivalent series of resistor and capacitor components installed in parallel [40].

Dielectricity occurs if an electric field is placed through a dielectric medium in which the strength of the electric field to pass through the medium is determined by the ability of the medium to be polarized in response to changes in the electric field [41]. Fig. 10 shows the dielectric constant and dielectric loss of the S1, S2, S3, and S4 membrane. The frequency-dependent dielectric constant indicates that the dispersion continuously increases at higher frequencies [42].

Fig. 10 shows that the dielectric constant of solid electrolyte

membranes of S1, S2, S3, and S4 was dependent upon the frequency. The dielectric constant value decreased exponentially with increasing frequency. Here, S4 membrane had the highest dielectric constant and dielectric loss; while, the S2 membrane had the lowest ones. Dielectric loss is the imaginary part of the permittivity as the amount of dissipative energy when entering an AC electric field or the amount of energy lost or dissipated [43].

The dielectric constant and dielectric loss at low frequencies are quite large due to strong dispersion. The low-frequency curve of the dielectric constant is a contribution of charge accumulation in the electrolyte and electrode interface areas [44]. The curve at high frequencies shows a decrease in the effect of frequency on the permittivity value caused by the periodic and rapid reversal of the electric field, resulting in no diffusion and vibration of the remaining ions [45]. The dielectric loss response of polymers depends on the polarity of the molecules at high frequencies. Fig. 11 portrays the comparison of dielectric loss values to dielectric constants.

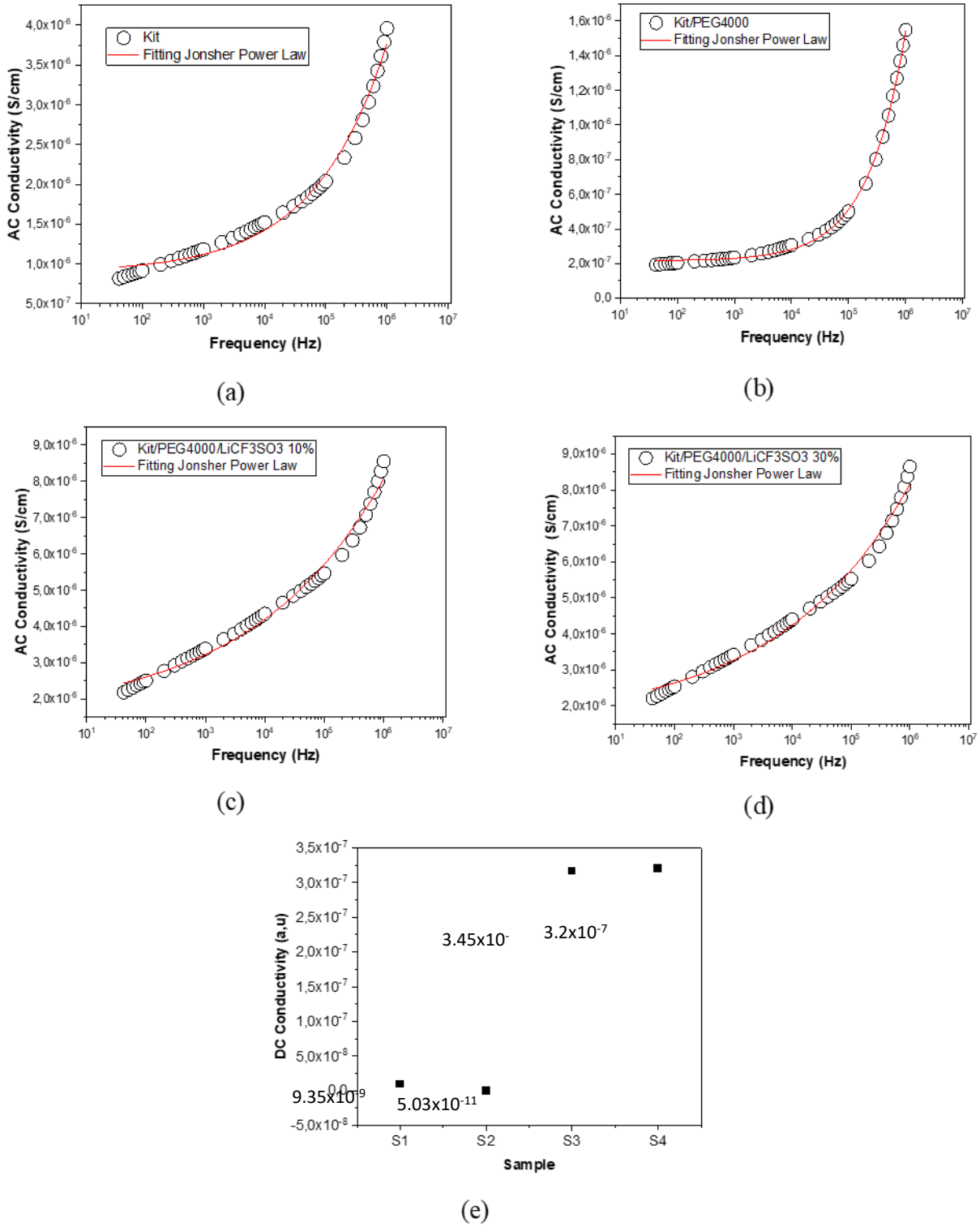

Fig. 8. Jonscher Power Law fitting for S1 (a), S2 (b), S3 (c), and S4 (d). DC conductivity of polymer solid electrolyte membrane (e)

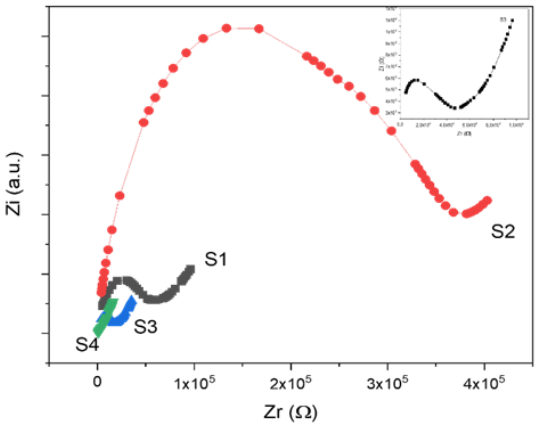

Fig. 9. Impedance of S1, S2, S3, and S4 membranes

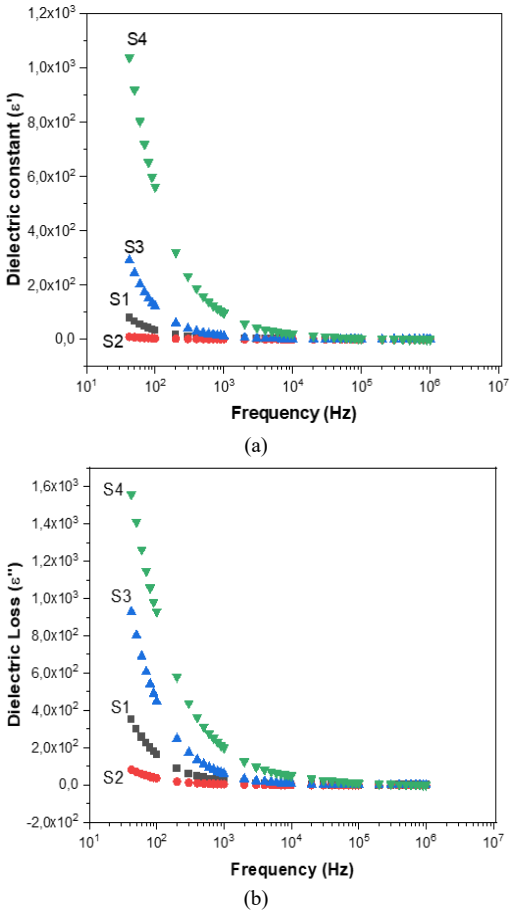

Fig. 10. Frequency-dependent plot of permittivity for S0, S1, S2, S3, and S4 membranes, (a) dielectric constant, (b) dielectric loss at RT

Fig. 11 illustrates the tangential loss and frequency of S1, S2, S3, and S4 membranes measured at room temperature by the loss tangent. At this point, the loss tangent tended to peak at low frequencies and remained constant at higher frequencies. The tangential loss, meanwhile, decreased at high frequencies due to the decrease in dipole polarization. The constant value at high frequencies decreased to adjust to the external electric field. Dipole relaxation in the sample caused peaks to appear at certain frequencies in chitosan. The characteristics of the dipole relaxation properties determined the strength and frequency of relaxation. The peak shifted to a higher frequency when $LiCF_3SO_3$ was added. Thus, it can be concluded that $LiCF_3SO_3$ contributes to an increase in segmental motion. This phenomenon exhibits the power of lithium triflate salt to accelerate segmental motion by increasing the free volume, thereby decreasing the relaxation time [46].

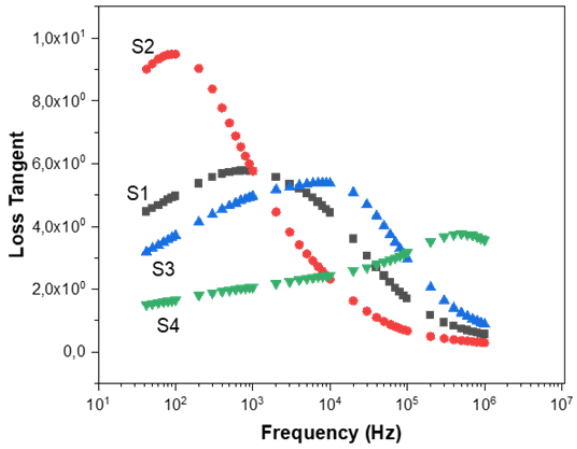

Fig. 11. Loss Tangent of S0, S1, S2, S3, and S4 membranes

4. Conclusion

The microstructural and electrical properties of the solid electrolyte polymer (SPE) membrane were significantly determined by the addition of chitosan/PEG4000/$LiCF_3SO_3$. The membrane's permittivity and ionic conductivity were boosted by $LiCF_3SO_3$, which also facilitated the transition to a semicrystalline structure, as evidenced by a reduction in crystallinity and an increase in lattice strain. Furthermore, the study identified the formation of a new functional group, SO_3, occurred due to the decomposition of $LiCF_3SO_3$ in the polymeric membrane. A constant value was reflected in the S-O bond related to the SO_3 functional group, as characterized by a strong atomic bond. The consistent dispersion of $LiCF_3SO_3$ throughout the chitosan/PEG4000 solid polymer electrolyte membrane has been proven by research, suggesting its potential utility as a solid electrolyte in secondary battery systems.

Acknowledgments

The Ministry of Education, Culture, Research and Technology (BRIN) in the Republic of Indonesia is gratefully acknowledged by the author. The funding for this research was provided by Universitas Jenderal Soedirman's "Riset Dasar Unsoed" grant.

References

1. F. A. Perdana, *Baterai Lithium*, *INKUIRI J. Pendidik. IPA*, 9 (2021) 113.
2. M. S. A. Rani, M. N. F. Norrrahim, V. F. Knight, N. M. Nurazzi, K. Abdan, and S. H. Lee, *A Review of Solid-State Proton–Polymer Batteries: Materials and Characterizations*, Polymers (Basel). 15 (2023) 1–27.
3. O. S. Burheim, *Engineering energy storage*. 2017.
4. J. Chattopadhyay, T. S. Pathak, and D. M. F. Santos, *Applications of Polymer Electrolytes in Lithium-Ion Batteries: A Review*, Polymers (Basel). 15 (2023).
5. S. Kaewpirom and S. Boonsang, *POLYMER Electrical response*

characterization of poly (ethylene glycol) macromer (PEGM)/ chitosan hydrogels in NaCl solution, 42 (2006) 1609–1616.

6. K. Sari, K. Abraha, Roto, Mashadi, and E. Suharyadi, *Effect of milling time on microstructures of nano-sized chitosan,* J. Phys. Conf. Ser., 1170 (2019).
7. K. Sari, S. Sunardi, A. B. S. Utomo, P. L. Toruan, E. Yulianti, and M. Mashadi, *Sifat Optik Dan Permitivitas Listrik Membran Polimer Padat Kitosan/Peo*, Sainmatika J. Ilm. Mat. Dan Ilmu Pengetah. Alam. 17 (2020) 97.
8. V. Koester, *Plasticizers – Benefits, Trends, Health, and Environmental Issues*, ChemViews. (2015) 1–9.
9. N. Yazie, D. Worku, N. Gabbiye, A. Alemayehu, Z. Getahun, and M. Dagnew, *Development of polymer blend electrolytes for battery systems: recent progress, challenges, and future outlook*, Mater. Renew. Sustain. Energy. 12 (2023) 73–94.
10. S. Kartika, S. Edi, Roto, and A. Kamsul, *Microstructures and functional group properties of nano-sized chitosan prepared by ball milling*. Mater. Sci. Forum. 948 (2019) 192–197.
11. Wicakso, D.R, M, Agus, A. Era, N, Nova Fitria, F, Firdaus, and F, Muhammad, *Potential of silica from water treatment sludge modified with chitosan for Pb(II)and color adsorption in sasirangan waste solution,* Commun. Sci. Technol. 7 (2022) 188-193.
12. L. Sampath Kumar, P. Christopher Selvin, and S. Selvasekarapandian, *Impact of lithium triflate (LiCF3SO3) salt on tamarind seed polysaccharide-based natural solid polymer electrolyte for application in an electrochemical device*, Polym. Bull. 78 (2021) 1797–1819.
13. Hossain, MD Sahadat, Ahmed, Samina, *Easy and green synthesis of TiO2 (Anatase and Rutile): Estimation of crystallite size using Scherrer equation, Williamson-Hall plot, Monshi-Scherrer Model, size-strain plot, Halder- Wagner Model*, Results in Materials. (2023) 100492.
14. S. Fatimah, R. Ragadhita, D. F. Al Husaeni, and A. B. D. Nandiyanto, *How to Calculate Crystallite Size from X-Ray Diffraction (XRD) using Scherrer Method*, ASEAN J. Sci. Eng., 2 (2022) 65–76.
15. M. Venkateswarlu, K. Narasimha Reddy, B. Rambabu, and N. Satyanarayana, *A.C. conductivity and dielectric studies of silver-based fast ion conducting glass system,* Solid State Ionics, 127 (2000) 177–184.
16. Sudaryanto, E. Yulianti, and H. Jodi, *Studies of Dielectric Properties and Conductivity of Chitosan-Lithium Triflate Electrolyte*, Polym. - Plast. Technol. Eng. 54 (2015) 290–295.
17. M. Schneider, P. Demoulin, R. Sussmann, and J. Notholt, *Fourier transform infrared spectrometry*, 10 (2013).
18. Q. Wang, N. Zhang, X. Hu, J. Yang, and Y. Du, *Chitosan/polyethylene glycol blend fibers and their properties for drug controlled release*, J. Biomed. Mater. Res. - *Part A*. 85 (2008) 881–887.
19. A. B. D. Nandiyanto, R. Ragadhita, and M. Fiandini, *Interpretation of Fourier Transform Infrared Spectra (FTIR): A Practical Approach in the Polymer/Plastic Thermal Decomposition*, Indones. J. Sci. Technol. 8 (2023) 113–126.
20. S. B. Aziz, T. J. Woo, M. F. Z. Kadir, and H. M. Ahmed, *A conceptual review on polymer electrolytes and ion transport models*, J. Sci. Adv. Mater. Devices, 3 (2018) 1–17.
21. S. B. Aziz *et al.*, *Characteristics of Methyl Cellulose Based Solid Polymer Electrolyte Inserted with Potassium Thiocyanate as K+ Cation Provider: Structural and Electrical Studies*, Materials (Basel). 15 (2022).
22. N. N. A. Amran, N. S. A. Manan, and M. F. Z. Kadir, *The effect of LiCF3SO3 on the complexation with potato starch-chitosan blend polymer electrolytes,* Ionics (Kiel). 22 (2016) 1647–1658.
23. S. Navaratnam, K. Ramesh, S. Ramesh, A. Sanusi, W. J. Basirun, and A. K. Arof, *Transport Mechanism Studies of Chitosan Electrolyte Systems*, Electrochim. Acta, 175 (2015) 68–73.
24. Costa, L.A.T, Goncalves, P.M, Cestarolli, D.T, Guerra, E.M, *Synthesis, intercalation reactions, and electrochemical studies for VO2/PEO/Chitosan*. 325 (2024) 129759.
25. S. Rajendran, R. Kannan, and O. Mahendran, *Ionic conductivity studies in poly(methyl methacrylate)-polyethylene oxide hybrid polymer electrolytes with lithium salts*, J. Power Sources, 96 (2001) 406–410.
26. S. Ramesh, T. F. Yuen, and C. J. Shen, *Conductivity and FTIR studies on PEO – LiX [X : CF 3 SO 3 −, SO 42 −] polymer electrolytes*, 69 (2008) 670–675.
27. K. Kumutha and Y. Alias, *FTIR spectra of plasticized grafted natural rubber-LiCF3SO3 electrolytes*, Spectrochim. Acta - Part A Mol. Biomol. Spectrosc. 64 (2006) 442–447.
28. Yang, Hui, Wu, Niangiang, *Ionic conductivity and ion transport mechanisms of solid-state lithium-ion battery electrolytes: A review,* Energy Sci. Eng. 10 (2022) 1643-1671.
29. A. A. Al-Tabbakh, N. Karatepe, A. B. Al-Zubaidi, A. Benchaabane, and N. B. Mahmood, *Crystallite size and lattice strain of lithiated spinel material for rechargeable battery by X-ray diffraction peak-broadening analysis*, Int. J. Energy Res. 43 (2019) 1903–1911.
30. F. Kingslin Mary Genova, S. Selvasekarapandian, N. Vijaya, S. Sivadevi, M. Premalatha, and S. Karthikeyan, *Lithium ion-conducting polymer electrolytes based on PVA–PAN doped with lithium triflate*, Ionics (Kiel)., 23 (2017) 2727–2734.
31. S. Islam, A. Siddika, N. Khatun, M. S. Hossain, M. H. A. Begum, and N. A. Ahmed, *Structural, dielectric and electric properties of manganese-doped barium titanate*. Int. J. Nanoelectron. Mater. 11 (2018) 419–426.
32. M. Toft, *The Effect of Crystalline Morphology on The Glass Transition and Enthalpic Relaxation in Poly (Ether-Ether-Ketone)*. Int. J. Nanoelectron. Mater. 2 (2011) 1–8.
33. A. Moradabadi and P. Kaghazchi, *Effect of lattice and dopant–induced strain on the conductivity of solid electrolytes: application of the elastic dipole method*, Materialia, 9 (2020) 100607.
34. K. Maryani, N. S. Anwari, W. N. Safitri, A. Hardian, E. D. Inggarwati, and A. Prasetyo, *The effect of synthesis temperature on structural, morphological, and band gap energy of plate-like Bi4Ti2.95V0.05O12 prepared by molten NaCl/KCl salt method*, Commun. Sci. Technol. 9 (2024) 1–6.
35. L. Schweiger, K. Hogrefe, B. Gadermaier, J. L. M. Rupp, and H. M. R. Wilkening, *Ionic Conductivity of Nanocrystalline and Amorphous Li10GeP2S12: The Detrimental Impact of Local Disorder on Ion Transport,* J. Am. Chem. Soc., 144 (2022) 9597–9609.
36. N. Wagner, *Electrochemical impedance spectroscopy," PEM Fuel Cell Diagnostic Tools*. 1 (2011) 37–70.
37. S. Chandra Dey *et al, Preparation, Characterization and Performance Evaluation of Chitosan As an Adsorbent for Remazol Red*, Int. J. Latest Res. Eng. Technol. (2016) 52–62.
38. O. G. Abdullah, R. R. Hanna, H. T. Ahmed, A. H. Mohamad, S. A. Saleem, and M. A. M. Saeed, *Conductivity and dielectric properties of lithium-ion biopolymer blend electrolyte based film*, Results Phys., 24 (2021) 104135.
39. K. Ashabul, K. Nita, S. Pirim, M. Supari, C. Sinta Anjas, and Z. Nafisatus. *Study in the impact of quaternized graphene oxide (QGO) composition as modifier on the chemical, physical, mechanical, and performance properties of polyvinylidene fluoride (PVDF)-based nanocomposite membrane.* Commun. Sci. Technol. 9 (2024) 30-37.
40. S. B. Aziz *et al.*, Impedance, *FTIR and transport properties of plasticized proton conducting biopolymer electrolyte based on chitosan for electrochemical device application*, Results Phys. 29 (2021).
41. A. S. Shaplov, R. Marcilla, and D. Mecerreyes, *Recent Advances in Innovative Polymer Electrolytes based on Poly(ionic liquid)s*, Electrochim. Acta. 175 (2015) 18–34.

42. L. Long, S. Wang, M. Xiao, and Y. Meng, *Polymer electrolytes for lithium polymer batteries*, J. Mater. Chem. *A*. 4 (2016) 10038–10039.
43. S. Navaratnam, A. Sanusi, A. H. Ahmad, S. Ramesh, K. Ramesh, and N. Othman, *Conductivity studies of biopolymer electrolyte based on potato starch/chitosan blend doped with LICF3SO3*, J. Teknol. 75 (2015) 1–5.
44. K. Sari *et al.*, *Effect of milling time on the microstructure and dielectric properties of chitosan nanopowder*, Int. J. Nanoelectron. Mater. 13 (2020) 1–8.
45. P. Parnasari, M. Nurhanisa, and B. S. Nugroho, *Studi Kapasitansi dan Konstanta Dielektrik Pada Karbon Aktif Tandan Kosong Kelapa Sawit,* Prism. Fis. 10 (2022) 98.
46. M. M. El-Nahass, A. F. El-Deeb, H. E. A. El-Sayed, and A. M. Hassanien, *Electrical conductivity and dielectric properties of bulk glass Se55Ge30As15 chalcogenide*, Phys. B Condens. Matter. 388 (2007) 26–33.